Received: 30 July 2020 | Revised: 18 December 2020 | Accepted: 26 January 2021

DOI: 10.1002/hyp.14066

RESEARCH ARTICLE

WILEY

Surface water-groundwater exchange dynamics in buried-valley aquifer systems

Corey D. Wallace[1] | Mohamad Reza Soltanian[1,2]

[1]Department of Geology, University of Cincinnati, Cincinnati, Ohio

[2]Department of Environmental Engineering, University of Cincinnati, Cincinnati, Ohio

Correspondence
Corey D. Wallace, Department of Geology, University of Cincinnati, Cincinnati, OH.
Email: wallacy@ucmail.uc.edu

Abstract

Groundwater is a primary source of drinking water worldwide, but excess nutrients and emerging contaminants could compromise groundwater quality and limit its usage as a drinking water source. As such contaminants become increasingly prevalent in the biosphere, a fundamental understanding of their fate and transport in groundwater systems is necessary to implement successful remediation strategies. The dynamics of surface water-groundwater (hyporheic) exchange within a glacial, buried-valley aquifer system are examined in the context of their implications for the transport of nutrients and contaminants in riparian sediments. High conductivity facies act as preferential flow pathways which enhance nutrient and contaminant delivery, especially during storm events, but transport throughout the aquifer also depends on subsurface sedimentary architecture (e.g. interbedded high and low conductivity facies). Temperature and specific conductance measurements indicate extensive hyporheic mixing close to the river channel, but surface water influence was also observed far from the stream-aquifer interface. Measurements of river stage and hydraulic head indicate that significant flows during storms (i.e., hot moments) alter groundwater flow patterns, even between consecutive storm events, as riverbed conductivity and, more importantly, the hydraulic connectivity between the river and aquifer change. Given the similar mass transport characteristics among buried-valley aquifers, these findings are likely representative of glacial aquifer systems worldwide. Our results suggest that water resources management decisions based on average (base) flow conditions may inaccurately represent the system being evaluated, and could reduce the effectiveness of remediation strategies for nutrients and emerging contaminants.

KEYWORDS

buried-valley aquifer, groundwater, heterogeneity, hyporheic exchange, riparian, spectral analysis, surface water-groundwater interactions, water quality

1 | INTRODUCTION

Surface water and groundwater are intimately connected along rivers, mixing within the sediments immediately beneath and adjacent to the channel (Epting et al., 2018; Martinez, Raiber, & Cox, 2015). Fluid flow across the riverbed and surrounding banks along short groundwater flow paths transports solutes between aquatic and riparian ecosystems, creating a zone with distinct physical, chemical, and biological properties relative to overlying surface water and deeper groundwater (Peralta-Maraver, Reiss, & Robertson, 2018). These flow paths define the hyporheic zone, a critical ecological transition area that controls the fate of nutrients and contaminants (Gandy, Smith, & Jarvis, 2007;

Lewandowski et al., 2011). Rivers may also receive groundwater contributions or lose water to the surrounding aquifer along larger-scale flow pathways, which can impact the finer patterns of hyporheic exchange (Harvey, Wagner, & Bencala, 1996; Trauth, Schmidt, Vieweg, Oswald, & Fleckenstein, 2015). Where this strong coupling between surface water features and groundwater systems exists, the exchange of water and solutes depends primarily on the hydraulic gradient between the two water bodies and the physical attributes (e.g., hydraulic conductivity [*K*]) of the surrounding sediments.

Hyporheic exchange patterns through glacial and postglacial sediments are often complex due to the highly heterogeneous nature of the deposits, within which *K* values often span several orders of magnitude (Miall, 1996). Fine, low-K facies (three-dimensional bodies of sediment [e.g., Liu et al., 2020; Soltanian & Ritzi, 2014; Wallace, Sawyer, Soltanian, & Barnes, 2020b]) can restrict or divert groundwater flow, while coarse, higher-*K* facies act as preferential flow pathways. Exemplary depositional environments for such complex sediment heterogeneity are glacial, buried-valley aquifers (Figure 1(a)), which formed wherever proglacial valleys drained large volumes of sediment and water away from ice margins (Erickson, Yager, Kauffman, & Wilson, 2019). In the United States alone, such aquifers underlie parts of 25 states and provide drinking water to nearly 43 million people (Johnson & Belitz, 2017, Yager et al. 2019).

The complex sediment heterogeneity of buried-valley aquifers may also influence the downstream transport of nutrients and contaminants, yet hyporheic processes and the fate of solutes in valley-fill sediments have been largely overlooked. Indeed, despite widespread anthropogenic contamination of glacial sediments in North America (Warner & Ayotte, 2014), much of the current research on buried-valley aquifers consists of stratigraphic knowledge based on over

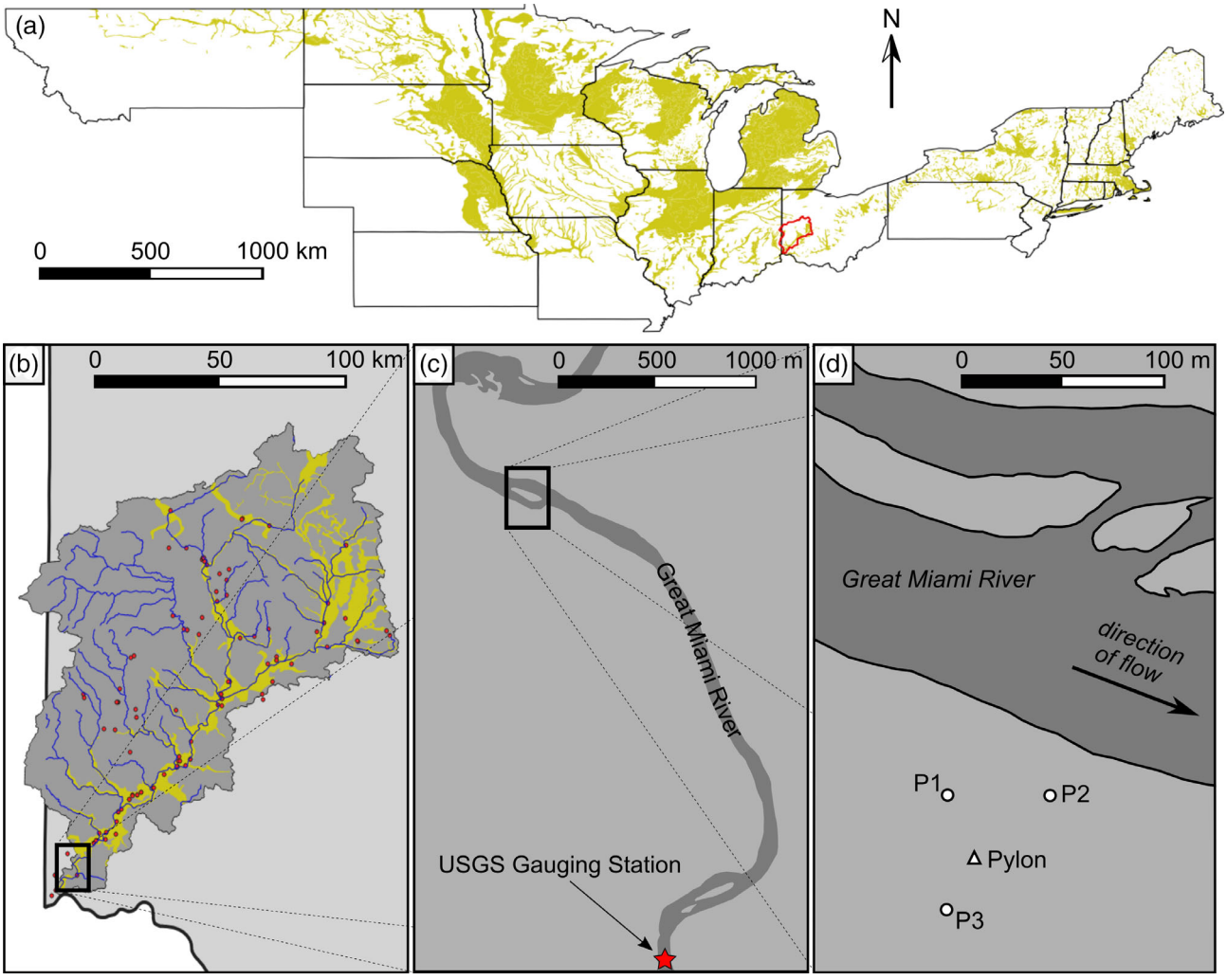

FIGURE 1 (a) Map showing the extent of the alluvial and glacial aquifers north of the southern-most line of glaciation in the conterminous United States. The great Miami watershed is outlined in red. (b) the great Miami watershed in southwestern Ohio. The great Miami Buried-Valley aquifer is shown in yellow, and major groundwater extraction wells are indicated by the red circles (c) the theis environmental monitoring and modelling site (TEMMS) is located along the south bank of the great Miami River approximately 28 km upstream of its confluence with the Ohio River. The USGS gauging station (indicated by the red star) is located roughly 3 km downstream of the study site. (d) Observation wells in the aquifer are indicated by the white circles, and the location of the data pylon is indicated by the white triangle

100 years of outcrop work and more than 50 years of subsurface water-well mapping (Cummings, Russell, & Sharpe, 2012). However, previous studies suggest that, even in varying geographic settings, buried-valley aquifers share similar mass transport characteristics, and thus a general understanding of the dynamics of surface water-groundwater interactions and nutrient transport should be widely applicable (Ritzi et al., 2002). Given the increasing importance of remediation strategies for emerging contaminants (e.g., 1,4-Dioxane, Per and polyfluoroalkyl substances [PFAS]), it is imperative to understand the small-scale processes that control transport and biogeochemical transformation within the hyporheic mixing zone and the adjacent riparian aquifer, without necessitating extensive excavation to characterize the subsurface heterogeneity. The goal of this work is to characterize surface water-groundwater dynamics within buried-valley aquifers using easily-monitored hydrogeologic parameters, and to identify potential implications for water quality. We seek to provide a conceptual model for the influence of glacial and postglacial sediments on nutrient and contaminant transport in buried-valley aquifers, especially in response to storm-events, which are the primary hydrologic forcing at our site. Using our conceptual model, we suggest management strategies associated with the remediation of emerging contaminants of environmental concern.

Extensive studies on the sedimentary architecture of buried-valley aquifers show that mud and diamicton facies juxtaposed with sand and gravel facies during periods of aggradation to create strongly bimodal heterogeneity (Ritzi et al. 2002; Titzel, 1997). A unique feature of buried-valley sedimentary architecture data is the presence of gravel-dominated facies such as open-framework gravel (OFG) cross-strata, which have negligible sand content and a unimodal grain size distribution (d_{50} > 2 mm). As a result, the conductivity of OFG facies can reach to up to 10^3 darcys (Ferreira et al., 2010; Jussel, 1989; Klingbeil, Kleineidam, Asprion, Aigner, & Teutsch, 1999; Lunt, Bridge, & Tye, 2004). The formation and preservation of OFG cross strata is common, especially along gravelly riverbeds (Lunt & Bridge, 2007), where they may strongly control hyporheic exchange by channelling flow wherever they intersect the channel boundary (Zhou, Ritzi, Soltanian, & Dominic, 2014). Further, quantitative field studies and numerical simulations have found that gravel-dominated facies tend to become hydraulically connected when they constitute one quarter to one third of the riverbed sediment volume, which could also promote flow through the adjacent riparian aquifer (Heinz, Kleineidam, Teutsch, & Aigner, 2003; Lunt et al., 2004; Zhou et al., 2014). In this study, we discuss the viability of detecting gravel-dominated facies using basic hydrologic measurements, and discuss the implications for nutrient and contaminant fate and transport.

Water temperature and specific conductance (SC) have long been used as conservative tracers to quantify the interactions between surface water and groundwater (Cox, Su, & Constantz, 2007; Harvey & Bencala, 1993; Kobayashi, Ishii, & Kodama, 1999; Palmer & Nadon, 1986; Runkel, 1998). Specifically, SC has been shown to be an effective tool for distinguishing preferential flow through the subsurface (Smith & Capel, 2018). When monitored continuously, water temperature and SC can also be used to differentiate hyporheic exchange volumes from discharges of water from somewhat deeper sources (Evans & Davies, 1998; Pilgrim, Huff, & Steele, 1979; Plummer et al., 2001). These measurements can also be used to approximate transport behaviour, but a comprehensive understanding of the transport of reactive solutes in groundwater requires knowledge of the interactions between the solute and the geologic media (Stollenwerk & Grove, 1987). Unfortunately, the novel transport characteristics of emerging contaminants are not well defined, and sampling in both river and groundwater is often difficult and costly. In the absence of the funding and technology required for regular monitoring, conservative tracers like temperature and SC may provide insight into where groundwater is most vulnerable to contamination. Here, we explore the predictive potential of basic hydrologic data for groundwater vulnerability, and discuss their implications for emerging contaminant transport within buried-valley aquifers. Though measurement of temperature and SC is not novel, our analytical framework provides a fundamental understanding of flow and transport dynamics that can be generally applied to glacial aquifers and other hydrologic systems subject to intimate surface water-groundwater interactions (e.g., riparian floodplains, coastal aquifers, dam-regulated rivers), and ensures that the methodology is readily imitable.

Continuous data sets of basic hydrologic parameters may also improve our understanding of water and solute flux through the hyporheic zone and riparian aquifer during hot moments, periods of enhanced flow and reactivity often related to storm events. The associated rise in river stage facilitates rapid infiltration early in the storm, which drives hydrogeochemical changes in the near-stream environment as solutes permeate the riverbed and floodplain (Sawyer, Kaplan, Lazareva, & Michael, 2014). As a result, storms dominate the solute export budget of many watersheds by enhancing nutrient fluxes and increasing microbial activity (Schilling, Li, & Zhang, 2006; Wondzell & Swanson, 1996; Zimmer & Lautz, 2014). It will be demonstrated in this work that such hot moments play a significant role in the geochemistry of buried-valley aquifers, where preferential gravel and OFG flowpaths may effectively distribute solutes through the groundwater, promoting increased nutrient transformation and making the aquifer more vulnerable to contamination. Here, we show the influence of hot moments on the hyporheic flow mixing as well as groundwater temperature and SC.

2 | STUDY AREA

The Great Miami Buried Valley Aquifer in southwestern Ohio (Figure 1) is an extensive buried-valley aquifer system that extends from Dayton to the Ohio River, about 20 km west of Cincinnati. It contains nearly 5.7 km^3 of water, and is the sole source of drinking water for over 3 million people. The majority of municipal groundwater extraction wells in the region are located in the aquifer (red dots in Figure 1(b)). Land use within the 9900 km^2 watershed is predominantly agricultural (~68%) and suburban (~18%). Sediment lithology consists primarily of sands and gravels with interbedded mud and diamicton facies. Sand and gravel layers can include channelized

outwash, outwash fans, and eskers, while mud and diamicton facies include till, loess, lacustrine deposits, debris flows, and overbank flood deposits (Ritzi et al., 2000). The aquifer averages roughly 3 km in width and 30–60 meters in depth, and aquifer transmissivity is estimated between 1200 and 3700 m^2 d^{-1}, with storativity of 0.2 (Spieker, 1968). The water table throughout the valley stands 5–15 m below the land surface and fluctuates between 1.5–5 m annually.

The field site (39.23755°N, 84.71252°W) is part of the Theis Environmental Monitoring and Modelling Site (TEMMS) established by the University of Cincinnati in 2017, and named after groundwater luminary Charles Vernon Theis. The study aquifer extends roughly 100 m into the southern bank of the Great Miami River approximately 28 km upstream of its confluence with the Ohio River (Figure 1). The 300 m^2 study aquifer is geometrically constrained by the surrounding bedrock valley, and the depth to bedrock at the study site averages 33 m. The average water table depth at the site is 5 m below the land surface. Bankfull channel width at the site averages 150 m and flow averages 110 m^3 s^{-1}. Mean annual precipitation is 990 mm. The channel of the Great Miami River is generally incised, but the floodplain is often inundated during the winter and spring when flows are greatest. Gravelly compound and point bars are prevalent within the channel and represent a larger scale of sedimentary architecture, within which planar and trough cross-bedded sand and planar cross-bedded gravel are common (Levy et al., 2011; Ritzi, Dai, Dominic, & Rubin, 2002).

3 | METHODS

3.1 | Sediment characterization

Three cores were collected from the field site during well installation to constrain floodplain hydrostratigraphy and sediment properties. Two cores were located immediately adjacent to the riverbank, and one was distally located about 100 m from the river (Figure 1(d)). Cores were collected using rotosonic drilling, which combines rotation with high frequency vibration to advance a core barrel to the desired depth. Once vibration is stopped, the core barrel is retrieved and the sample is extracted. Cores were extracted from the ground surface to the underlying bedrock in 150 cm intervals, and were immediately sealed and stored until analysis.

Cores were visually described for mineral composition, colour, and grain size at 5 -cm resolution. Based on visual descriptions, 10 representative intervals were selected from each core (30 samples total) and analysed for grain size and mineral content. Grain size was analysed for sediments within the range 0.037–8 mm using a Gilson SS-15 Sieve Shaker. All of the samples but one had sediments larger than 8 mm, which were further classified to grains sized less than 80 mm. Mineral composition and the proportion of minerals present were determined using X-ray powder diffraction (XRD). Minerals were identified by measuring the distances between the planes of atoms that constitute the sample by applying Bragg's Law (Bragg, 1913):

$$n\lambda = 2d\sin\theta, \quad (1)$$

where n is the order of the diffracted X-ray bean, λ is the wavelength of the incident beam, d is the distance between adjacent planes of atoms, and θ is the angle of incidence of the X-ray beam. Each characteristic set of d-spacings provides a unique mineral identifier used to determine the presence and proportion of each mineral in the sample.

3.2 | Groundwater and Hyporheic exchange

Six observation wells were installed within the floodplain to monitor groundwater levels and basic water quality parameters (temperature, SC), consisting of two adjacent wells (one shallow, one deep) at three triangularly-spaced locations (Figure 1(d)). Wells were constructed of PVC with 11.5 cm o.d. and were screened in 3 m intervals, with the shallow and deep well screens positioned between 6–9 m and 27–30 m below the ground surface, respectively. Multiparameter sensors (YSI 600LS) were deployed inside each well to monitor hydraulic head, temperature, and SC at 15-min intervals. Data was continuously monitored from February 23, 2017 through December 31, 2019. A central pylon houses a thermometer and hygrometer to collect data on ambient atmospheric conditions, and a telecommunications link that transmits data from the site every 15 minutes (Figure 2). River stage was acquired from a nearby USGS gauge (#03274615) located roughly 3 km downstream of the site. Hyporheic exchange was calculated using Darcy's law between the river and riparian aquifer at each location. Exchange in both the shallow and deep wells was calculated to infer vertical variations in sediment stratigraphy. For each of the monitoring wells, the aquifer response to changes in river stage was quantified by cross-correlating the water table elevation and river stage and computing the lag time.

The general direction of groundwater flow is estimated through time by a three-point solution that calculates the hydraulic gradient vector (direction and magnitude) from the coordinates of the three wells and their associated hydraulic head measurements. Thus, the groundwater flow direction will depend on the magnitude of K and the orientation of the hydraulic gradient. The method assumes an effective aquifer K of 82.3 m d^{-1} (Spieker, 1968) to calculate the horizontal direction and magnitude of groundwater flow at both shallow (6–9 m) and deep (27–30 m) sensor depths. Though this assumes horizontal isotropy in aquifer material properties, differences in the hydraulic gradient vector with depth can indicate depth-related changes in both sediment conductivity and tortuosity. For example, a larger magnitude flow at 27 m depth that is offset 10° from the flow direction at 6 m could indicate that shallow sediments are less permeable and that confining layers are diverting groundwater flow. Variations in the hydraulic gradient vectors through time are plotted on a rose diagram, a circular frequency histogram commonly used for directional (azimuthal) data to show the frequency of occurrence of flow direction recorded over a given period. Flow rose diagrams were created for a number of episodic flow events during each year of record, which were compared against diagrams that represent base flow conditions.

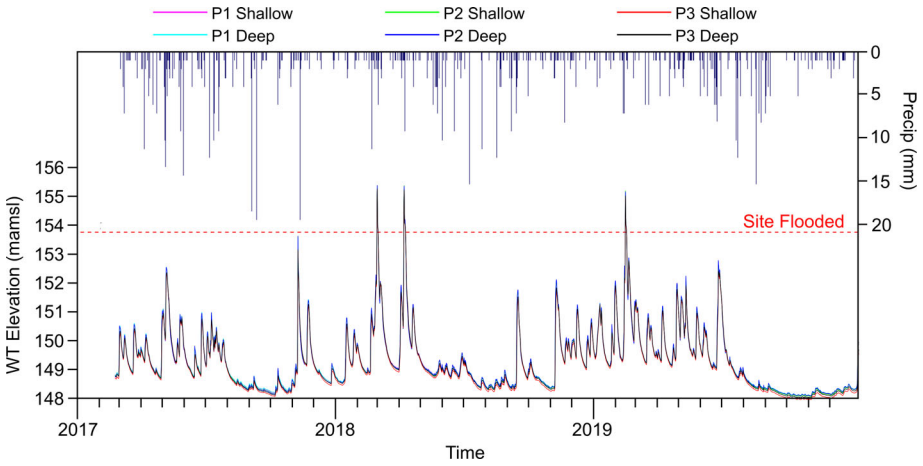

FIGURE 2 Water table elevation (shown) and basic water quality parameters (i.e., temperature and specific conductivity; not shown) were continuously monitored throughout the TEMMS aquifer at locations P1, P2, and P3. The water table was highly responsive to changes in river stage caused precipitation, and the floodplain was inundated three times during the study period (indicated by the red dashed line). TEMMS, theis environmental monitoring and modelling site

3.3 | Temporal analysis

Spectral analysis is a powerful tool in hydrologic science for its ability to quantify the links between hydrologic perturbations and conditions within the aquifer. Its power lies in its ability to decompose a time-series into its component frequencies, which can then be related to the frequency of hydrologic events. Further, by evaluating a continuously measured aquifer response to environmental variations, spectral analysis can effectively explain their influence across multiple timescales. Fourier-transform-based spectral analysis and other filtering techniques have had some practical applications in hydrology (e.g., Fleming, Lavenue, Aly, & Adams, 2002; Sang, Wang, & Liu, 2012; Schaefli, Maraun, & Holschneider, 2007), but their potential for comprehensively analysing hydrologic time-series has not been fully realized. Care must be taken to choose an appropriate transfer function, however, as misinformed application can lead to misinterpretations of the data (Du, Zhao, & Lei, 2017; Schuite, Flipo, Massei, Rivière, & Baratelli, 2019).

Spectral analysis such as the continuous wavelet transform (CWT) characterizes the general frequency content of time-series data, and resolves temporal variations in energy at a given frequency related to hydrologic events. Further, comparison of different CWT signals can help identify relationships between time series and provide information about signal lag. The CWT of a signal X_n is defined as (Farge, 1992; Grinsted, Moore, and Jevrejeva, 2004):

$$W_n^X(s) = \sqrt{\frac{\delta t}{s}} \sum_{n'=1}^{N} X_{n'} \psi_0 \left[(n'-n) \frac{\delta t}{s} \right], \quad (2)$$

where s is the scale of the transformed time-series $W_n^X(s)$, n is time, and n' is reversed time. Here, we used the Morlet wavelet because it is well-localized in space and time, and is defined as:

$$\psi_0(\eta) = \pi^{-1/4} e^{i\omega_0 \eta} e^{-\eta^2/2}, \quad (3)$$

where ω_0 is dimensionless frequency (ω_0 = 6) and η is dimensionless time. Edge effects cause errors at the beginning and end of the wavelet power spectrum, indicated by the shaded regions in CWT images. The CWT reveals when particular frequencies in a time-series are stronger or weaker, and has been successfully used to resolve the effects of hydrologic perturbations across temporal scales (e.g., Wallace, Sawyer, & Barnes, 2019). For example, if a sudden rise in river stage following a storm affects SC over 1 week, the wavelet plot of SC shows higher power at the one-week frequency during that time. We analysed hydraulic head, temperature, and specific conductivity data using CWT analysis, and computed the phase lag between signals to determine how perturbations propagate through the riparian aquifer. Inter-well comparisons of the CWT for all three variables were used to identify variability within the floodplain, while comparisons of hydraulic head between each well and the river provide insight into the variability of hyporheic exchange.

4 | RESULTS

4.1 | Hydrostratigraphy

The riparian aquifer lithologic sequence typically includes a sandy gravel base with interbedded OFG facies overlain by ~1 m thick, dark organic-rich silt and clay deposits, interpreted as till (Norris & Spieker, 1966; Spieker, 1968) (Figure S1). The lower units at all three locations are poorly sorted and subrounded, ranging in size from cobbles to medium sand with trace amounts of clay (Figure S2). Grains are predominantly quartz, with some carbonaceous minerals including calcite and some silicate minerals including chlorite. Intermittent OFG cross-strata constitute roughly 5% of the sediment column, wherein cobbles are typically >5 cm. The overlaying silt and clay layers are well-sorted, with grains consisting predominantly of phyllosilicate minerals including illite, kaolinite, and smectite. The base of the aquifer immediately above the bedrock is a limy clay layer primarily composed of chlorite and illite.

4.2 | Hydrologic exchange

Net flux was away from the river at baseflow conditions (the river was losing), but episodic, high-flow (i.e., storm) events changed the

local hydraulic gradient and drove flux across the riverbed and bank (Figure 3). During such events, the magnitude of water table response to fluctuations in river stage decayed with distance into the riparian aquifer. Average amplitudes of water table fluctuations were 63%, 67%, and 51% of the river stage amplitude at locations P1, P2, and P3, respectively. Generally, surface water infiltration into the riparian aquifer began approximately 1–2 h after river stage increased. Water table data for each monitoring well indicate that water levels lag in time from the river stage, with inter-annual variability at each location. The average lag time was similar near the river at locations P1 and P2 (located 56 meters and 36 meters from the riverbank, respectively), ranging from 4.4 to 8.9 h and 5.5 to 7.3 h, respectively. At roughly twice the distance into the aquifer (95 meters from the streambank), the average lag time at location P3 ranged from 8.5 to 10.3 h. Within each monitoring well, the water table response at the shallow sensor consistently lagged the response at the deeper sensor by 37 ± 17 min, with the shortest average lag at P1 (30 min) and the longest at P3 (45 min).

Based on Darcy's law, the instantaneous flow rate across the sediment–water interface ranged from −5.84 to 1.07 m d^{-1} in 2017, from −4.59 to 1.58 m d^{-1} in 2018, and from −3.92 to 1.79 m d^{-1} in 2019. In general, exchange fluxes were greater through the shallow aquifer where the hydraulic gradient was steeper across the bank seepage face. Near the riverbank, the volumes of water infiltrating and exfiltrating were approximately equal at P1, but infiltration dominated (∼60% of the total exchange volume) at P2. Further into the aquifer at location P3, only about 25% of groundwater flow was toward the river, indicating that the river is predominantly losing and that the near-river riparian aquifer is a local zone of increased surface water-groundwater mixing.

Rose diagrams reveal similar groundwater flow patterns during baseflow conditions over all 3 years (Figure 3(g–i)). The flow azimuth in the shallow aquifer averaged 170.6°N and varied by less than 5%, while the average flow direction of 164.4°N in the deeper aquifer was more variable, changing nearly 20% between annual baseflow seasons. This similarity is likely associated with aquifer sediment lithology, where high-*K* facies (i.e., gravelly sand and OFG) consistently channel infiltrating surface water along the same preferential flowpaths. In contrast, the direction and magnitude of groundwater flow in the shallow and deep aquifer were highly variable during episodic flow events, showing changes even between back-to-back storm events within the same year. Flow direction varied by up to 43% in the shallow aquifer, and by nearly 75% in the deeper aquifer.

4.3 | Water quality

The mean water temperature in 2017 was 17.81 °C, 16.09 °C, and 14.99 °C with a maximum value of 20.21 °C, 22.20 °C, and 16.50 °C and a minimum value of 16.39 °C, 11.73 °C, and 14.11 °C at locations P1, P2, and P3, respectively. The mean water temperature in 2018 was 15.86 °C, 17.02 °C, and 13.88 °C with a maximum value of 18.71 °C, 21.34 °C, and 18.47 °C and a minimum value of 9.53 °C, 6.87 °C, and 5.41 °C at locations P1, P2, and P3, respectively. The mean water temperature in 2019 was 14.39 °C, 15.54 °C, and 12.78 °C with a maximum value of 16.53 °C, 19.43 °C, and 14.50 °C and a minimum value of 7.44 °C, 4.38 °C, and 2.09 °C at locations P1, P2, and P3, respectively. Overall, the water temperatures measured at P3 were less variable ($\bar{\sigma}$ = 0.82 °C) than those measured at P1 ($\bar{\sigma}$ = 0.95 °C) and P2 ($\bar{\sigma}$ = 2.41 °C). Less hyporheic exchange farther from the river-aquifer interface likely maintains relatively stable water temperatures at P3, while at P2 closest to the river, the water temperature was significantly more variable.

The average SC of the Great Miami River over the study period was 685.4 ± 154 μS cm^{-1}. In the shallow aquifer, average SC was 702.9 ± 27.9, 699.4 ± 43.7, and 763.1 ± 94.5 μS cm^{-1} at locations P1, P2, and P3 respectively. In the deep aquifer, average SC was 699.1 ± 18.8, 728.8 ± 34.1, and 475.6 ± 70.0 μS cm^{-1} at locations P1, P2, and P3 respectively. Values were relatively consistent temporally and with depth at wells P1 and P2, likely due to their proximity to the river-aquifer interface. Consistent exchange with the river also reduced variability around the mean to just 3.3% and 5.5% at P1 and P2, respectively. Conversely, SC values at P3 differed by nearly 60% with depth, and showed larger fluctuations (12.4% about the mean) through time. Average SC throughout the aquifer was highest in the shallow aquifer at P3, which typically only becomes saturated following stage rise due to storm events. As such, the shallow flowpaths at this location are more influenced by surface water infiltration than regional groundwater flow. Deeper into the aquifer, SC values are low relative to the rest of the aquifer, indicating a heavier groundwater influence and limited exchange with surface water.

4.4 | Temporal dynamics

Storms governed changes in water table elevation throughout the year, but their influence on SC and temperature was moderated by seasonal variations. Water table dynamics were comparable at all locations and depths due to the high aquifer permeability and connectivity with the river. The largest responses were seen over several days following large storm events, with minimal changes during the winter when river stage is lowest and least variable (Figure 4). Temperature patterns were also relatively consistent between wells, with the largest temperature variations occurring in early spring when cold surface water infiltrates and mixes with more temperate groundwater. The surface water and groundwater are roughly the same temperature for the rest of the year, however, so the temperature signal showed few other perturbations despite the mixing indicated by SC data. Spatial and temporal variations in temperature have important implications for microbial reaction kinetics, which are sensitive to both temperature and nutrient availability. Though SC dynamics were also generally comparable between locations, a notable difference in the CWT of the SC signal occurred in late 2017. A large storm event in early November drove changes in the water table elevation at all locations. While the SC response at P1 near the bank was moderately low (wavelet power < 10), the concurrent response at P3 was significant

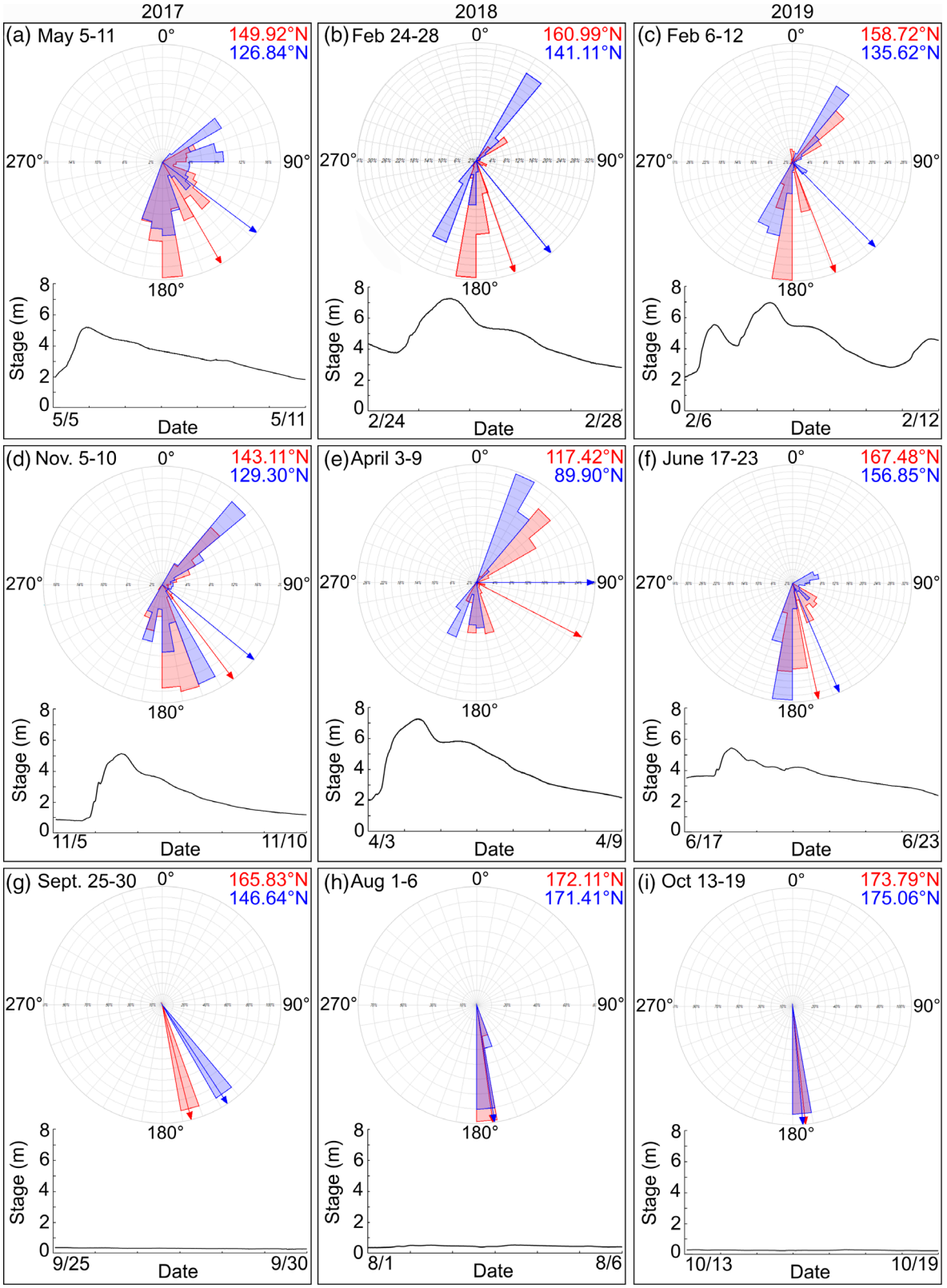

FIGURE 3 Rose diagrams showing flow variability in 2017 (left column), 2018 (middle column), and 2019 (right column). Episodic flow events caused by storms (a-f) strongly influenced both the shallow (red) and deep (blue) hydraulic gradient, and flow direction and magnitude varied at each location even within the same year. Flow during baseflow conditions (g-i) also shows variability in both the shallow and deep aquifer which likely correspond to geomorphic changes in the streambed and aquifer

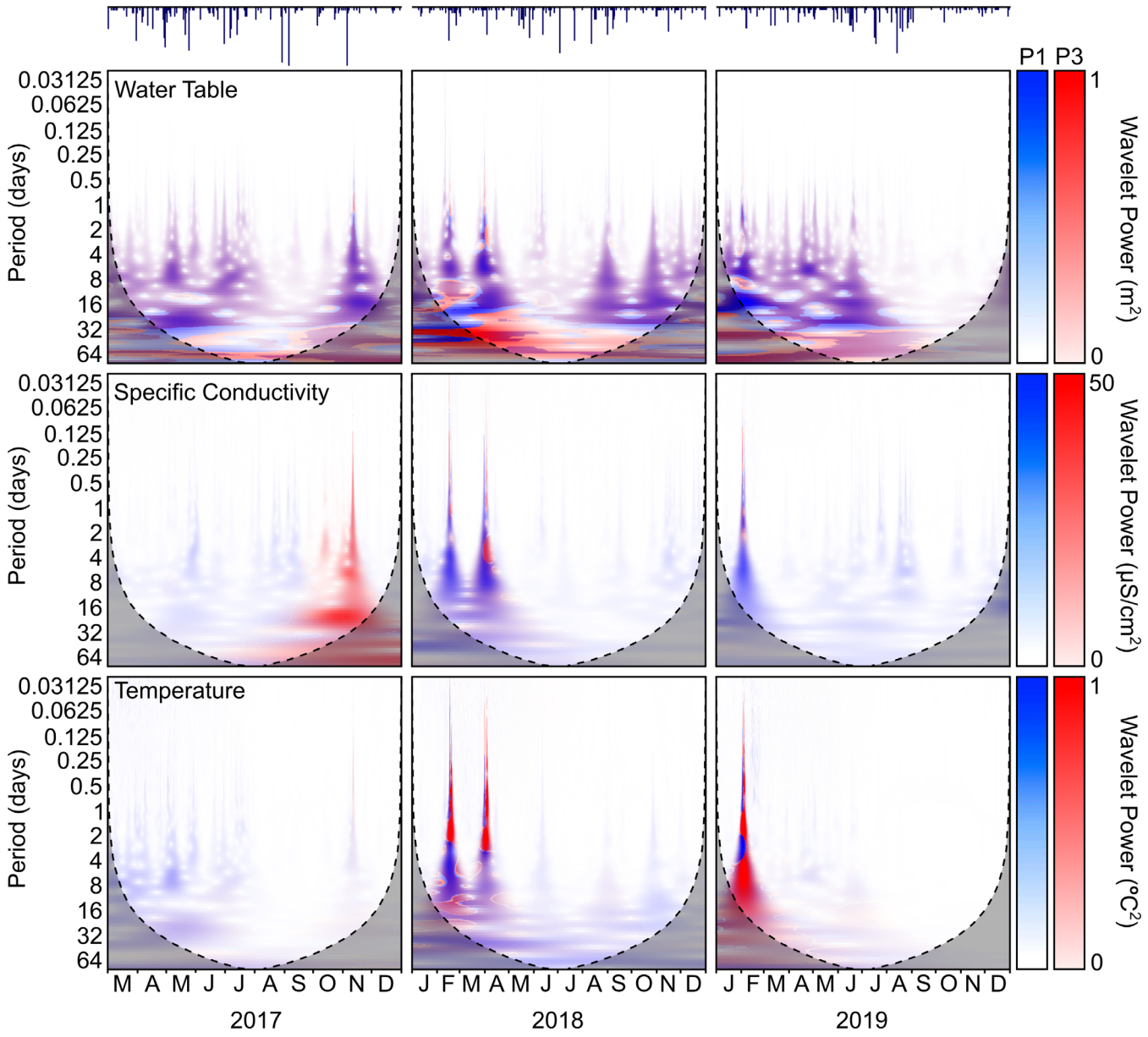

FIGURE 4 Continuous wavelet transformation of the water table (top), specific conductivity (middle), and temperature (bottom) data at wells P1 (blue) and P3 (red). An inverted hyetograph above each column indicates timing of large storms. Signals at each location often displayed similar frequency content, indicated by the blending of their respective colours in regions with high magnitude. A notable exception was seen in the 2017 specific conductivity signals, which showed considerable power at longer periods at P3 while concurrently almost no signal was seen at P1

(wavelet power > 50) over periods of 0.5 to 16 days. This important spatial difference demonstrates how the complex sedimentary architecture of glacial aquifers controls the timing and distribution of subsurface solute delivery.

5 | DISCUSSION

5.1 | Hydrologic response to stage fluctuations

Spatial variations in stratigraphy undoubtedly affect hyporheic exchange and groundwater flow patterns in buried-valley aquifers. Water table response to river stage fluctuations not only decayed with distance into the aquifer, but response time varied vertically between adjacent shallow and deep sensors. Signal variation at each location can correlate to the physical characteristics of each sediment column, which are bracketed by the adjacent shallow and deep sensors. Sediment cores at each location show that, within this interval, intermittent silt and clay layers extend through the bulk sand and gravel facies. Where they exist, the lower-*K* facies range from 0.05 to 0.25 meters in thickness and form barriers to vertical flow. Though the lateral extent of these layers is not clear, their presence compounds upon the complex flow regime by creating tortuous flowpaths through the aquifer. Such layering could also help

explain the high variability observed in flow direction and magnitude during storm events.

At each location, anisotropy in floodplain stratigraphy also influences preferential flow patterns: sand and gravel layers allow nutrient-rich river water to penetrate farther into the riparian aquifer than impermeable silt layers. This was evidenced at our site by the response of groundwater temperature and SC to rapid changes in river stage during storm events. Groundwater temperature decreased while SC increased in response to the infiltration of cold river water (many storms occurred in late winter and early spring), but the response at each location (i.e., P1, P2, P3) was tempered by the magnitude of stage rise. During shorter storms of lower magnitude, the temperature and SC were only impacted near the river bank (location P2 in our site), indicating that surface water did not travel far inland. Conversely, large storms that caused a sudden, significant rise in stage lowered temperature and SC throughout the aquifer. The similarity in the magnitude and timing of the conductivity response at each location indicates rapid flow through the subsurface, likely along preferential flowpaths created by connected OFG and gravelly sand facies.

At each location, the responses of temperature and SC in the deeper aquifer were damped relative to the shallow aquifer. During all but the largest storm events, the signals in the deeper aquifer showed roughly half the variation of those in the shallow aquifer. Further, temperature and SC in the deeper aquifer often recovered several hours sooner following perturbations. Thus, it is likely that the deeper aquifer is more groundwater-dominated while the shallow aquifer is more influenced by the river. Given the importance of hydrostratigraphy for hyporheic exchange and groundwater flow processes, measured fluxes at the study site may be representative of a significant portion of buried-valley aquifers. The geology at our site is generally consistent with geologic descriptions of buried-valley aquifers around the world (layered sand and gravel facies overlain by clays and silts) (Cumming et al., 2012; Dragon & Gorski, 2009; Ritzi, Jayne, Zahradnik, Field, & Fogg, 1994).

5.2 | Impacts of hot moments on riverbed conductivity

Inter-annual variability in groundwater flow direction and magnitude is likely associated not only with the magnitude of stage rise during storms, but also spatial and temporal variations in riverbed conductivity. We saw evidence of variable riverbed conductivity in our rose diagrams, which showed changes in the groundwater flow regime between storm events even within the same year. Throughout much of the year, fine sediments carried by infiltrating river water block pore spaces and clog the riverbed (Wojnar, Mutiti, & Levy, 2012). During storm events, scour may cleanse the riverbed of its clogging by removing fine sediments, thereby increasing *K* and connection with the adjacent riparian aquifer (Levy et al., 2011). As a result, preferential flowpaths may become less conductive at the stream-sediment interface as their connection with the channel changes, shifting the orientation and magnitude of infiltrating surface water. This phenomenon was observed at our site through inter-annual variations in water table response throughout the aquifer. For instance, during storm events that raised the river stage by >1 meter, the average amplitudes of water table fluctuations relative to river stage amplitude at locations P1, P2, and P3 varied significantly between years (Table 1).

TABLE 1 The average amplitude of water table fluctuations as a percentage of river stage amplitude during storms that raised the stage by >1 meter. Response throughout the aquifer varied between years, related both to the magnitude of stage rise and changes in riverbed conductivity

Year	No. of storms	P1 response	P2 response	P3 response
2017	36	57.2%	58.7%	45.4%
2018	29	63.7%	67.7%	50.6%
2019	17	67.6%	70.4%	57.6%

This also has implications for solute transport, evidenced at our site by changes in SC during individual storm events. Infiltrating river water lowered groundwater SC concentrations, with consistently larger changes at location P1 than P2, but the magnitude of change was variable. For example, SC dropped by 58% and 48% at P1 and P2, respectively, during the first major storm event of 2018 (Figure 3(b)), and then by 61% and 58% at P1 and P2, respectively, during a storm event less than 2 months later (Figure 3(e)). During the same two storm events, SC at location P3 dropped by 51% and 36%, respectively. These results imply that, even over a short timescale, changes to riverbed conductivity during hot moments can alter flow pathways and the efficiency of solute transport. It is thus crucially important, both in buried-valley type watersheds and in other similar hydrologic systems containing high-*K* sediments, that the connectivity and exchange rates between surface water and groundwater bodies be regularly assessed to maintain an understanding of the system dynamics. While this unclogging phenomenon during the rising limb of the river stage can change the riverbed conductivity, most scour events remove only the transient sediments, and thus only increase the vertical *K* by a factor of 1.5 (Levy et al., 2011; Mutiti & Levy, 2010). Nevertheless, its effect should not be neglected in dynamic systems with intimately connected surface water and groundwater bodies, especially when regular hydrologic perturbations disrupt the baseflow regime.

5.3 | Significance of gravel-dominated facies on hyporheic exchange

Gravel-dominated facies such as OFG are significantly more permeable that their surrounding sand and gravel counterparts, and thus their presence and distribution should influence the magnitude and direction of hyporheic exchange. Such OFG cross-strata are quite common in buried-valley aquifers, and the resulting preferential flow pathways are persistent and distributed throughout the sedimentary

architecture. The low proportion of OFG facies observed within the sediment cores at our site indicates that the pathways are likely not fully-connected as per percolation theory (e.g. Guin & Ritzi, 2008; Stauffer & Aharony, 1994; Wallace et al., 2020b), but even some connection within the aquifer could be significant. Permeable gravel layers adjacent to OFG facies could also serve as intermediary preferential flowpaths, effectively increasing the connectivity of OFG throughout the aquifer.

The locations where OFG strata intersect the river channel also play an important role, as preferential flow may only occur along some flowpaths once the river reaches a certain stage height during storm events. Channel intersection of such OFG strata does not explicitly signify that hyporheic exchange will be affected, but rather that the unit represents a significant avenue of exchange under the right conditions. However, because each storm event generates different river flow dynamics, flux across the sediment–water interface varies by event and induces divergent groundwater flow regimes throughout the aquifer. Thus, despite the stationarity of connected OFG cross-strata within the sedimentary architecture, differing flow patterns emerge based on the river stage and its impact on the local hydraulic gradient.

5.4 | Conceptual model of solute transport through buried-valley aquifers

The complex internal structure and interconnectedness of permeable facies has implications for mass transport and removal (i.e., nitrate, emerging contaminants) within buried-valley aquifers. Under base flow conditions at our site, river discharge is relatively static and the subsurface hydraulic gradient slopes away from the river. River discharge and velocity increase on the rising limb of the storm hydrograph, and the Darcy flux away from the channel also increases. Solutes that enter the banks are routed along preferential flowpaths and transported laterally and vertically as the water table rises, where they may be transformed as they are exposed to microbially-active sediments. Though this process is consistent in the majority of riparian aquifers, the sparsity of impermeable silt layers and the presence of highly conductive cross-strata such as OFG create the potential for increased degradation within buried-valley aquifers, as solutes are efficiently transported along pathways several orders of magnitude more permeable than sand or gravel. On the falling limb of the storm hydrograph, bank release begins and water exfiltrates into the channel, with greater Darcy flux from the shallow aquifer where the hydraulic gradient is steepest. Exfiltrating water should be chemically different from surface water as a result of these subsurface transformations. Though the inland solute transport distance and extent of chemical transformation is strongly influenced by the spatial variability in hydraulic and chemical attributes which arises from the aquifer sedimentary architecture and the magnitude of stage fluctuations, this pattern is likely consistent in buried-valley aquifers given their similar mass transport characteristics.

The impermeable bedrock walls surrounding the narrow, elongated buried-valley restrict lateral flow to the aquifer, which limits exchange with deeper groundwater. Thus, the majority of groundwater flow originates from the river. The tight connection between river water and groundwater makes buried-valley aquifers among the most productive aquifers in the world, but also makes them vulnerable to groundwater contamination. Preferential flowpaths, like those created by connected gravel facies (e.g., OFG cross-strata), are especially vulnerable sites because they efficiently transport contaminated river water into the aquifer. Further, direct bank infiltration along the river channel undermines the potentially protective role of silt and clay layers that overlay the deeper sandy gravel sediments, which could otherwise limit vertical exchange and prevent contaminant infiltration to the aquifer. This tight connection between surface water and groundwater bodies would also prove significant in systems with regular stage fluctuations (i.e., tides, dam release), however, as stage-induced mixing drives solute transport and bolsters degradation rates (e.g., Wallace et al., 2020a, Wallace et al., 2020b).

At our site, observation wells near the river-aquifer interface experienced the most hyporheic exchange and showed temperature variations similar to river water. Specific conductance is representative of conservative solutes, but also indicates the subsurface flow patterns other reactive contaminants are likely to follow. The rapid SC signal response at P1 and P2 during storm events underscores the hydraulic connectivity of the river and groundwater near the river, where the high volume of river water-groundwater exchange supplies nutrients for microbial transformation. However, episodic and seasonal changes in groundwater temperature related to river water temperature dynamics near the river would effectively reduce reaction rates, suggesting that nutrient transformation is least efficient where loads are greatest. Based on the temperature signal, location P3 was less influenced by stage changes, and groundwater flow remained away from the river the majority of the time. The shallow aquifer at this location showed elevated average SC values, however, which are indicative of surface water influence. Considering the relatively steady temperature signal, and using SC as a proxy for nutrient delivery, the shallow aquifer further from the river is likely a more optimal location for efficient microbial transformations. Even in buried-valley aquifer systems where flow is predominantly toward the river, microbial reaction hotspots likely localize along preferential flowpaths located far enough from the stream-aquifer interface to modulate temperature variation.

6 | CONCLUSIONS

Most groundwater remediation strategies and water resources management decisions are based on flow and nutrient delivery patterns during average, base flow conditions, often due to the cost and difficulty of obtaining accurate measurements during floods or storm events. However, our findings suggest that, both in buried-valley aquifers and other similar hydrologic systems, neglecting the effects of hot moments could significantly alter the appropriate water

management response. Not only do large flow events affect the direction and magnitude of groundwater flow during the event, but they may also alter the geomorphic state of the river channel and shallow aquifer, altering the distribution of preferential flowpaths which deliver nutrients to the subsurface. As a result, the distribution of reaction hotspots likely shifts over short timescales. Thus, basing water resources management decisions on base flow analyses inaccurately represents the system being considered, and could reduce the effectiveness of remediation strategies for contaminants of emerging concern.

ACKNOWLEDGEMENTS

This research was supported by the National Science Foundation (EAR-PF 1855193). The Theis Environmental Monitoring and Modelling Site was built with funding from the University of Cincinnati, the Duke Energy Foundation, and the Miami Conservancy District on land provided by Great Parks of Hamilton County. Mike Ekberg and the Miami Conservancy District graciously provided stage and water quality data for the Great Miami River. We thank David Nash for designing the publicly-available data interface for the site, which provides real-time readings of hydrologic conditions at the site. The free tool is available online at https://cvtheisgwo.artsci.uc.edu/. This manuscript benefited from the constructive feedback of two anonymous reviewers.

DATA AVAILABILITY STATEMENT

All hydraulic head, temperature, and specific conductivity data are available on CUAHSI'S HydroShare site (https://doi.org/10.4211/hs.2a7eafc820954faba2db53836f24382e).

ORCID

Corey D. Wallace https://orcid.org/0000-0001-7240-0319

REFERENCES

Bragg, W. H., & Bragg, W. L. (1913). The reflection of X-rays by crystals. *Proceedings of the Royal Society*, *88*, 428–438. https://doi.org/10.1098/rspa.1913.0040

Cox, M. H., Su, G. W., & Constantz, J. (2007). Heat, chloride, and specific conductance as ground water tracers near streams. *Groundwater*, *45* (2), 187–195. https://doi.org/10.1111/j.1745-6584.2006.00276.x

Cummings, D. I., Russell, H. A. J., & Sharpe, D. R. (2012). Buried-valley aquifers in the Canadian prairies: Geology, hydrogeology, and origin. *Canadian Journal of Earth Science*, *49*, 987–1004. https://doi.org/10.1139/E2012-041

Dragon, K., & Gorski, J. (2009). Identification of hydrogeochemical zones in postglacial buried valley aquifer (Wielkopolska buried valley aquifer, Poland). *Environmental Geology*, *58*, 859–866. https://doi.org/10.1007/s00254-008-1561-0

Du, K., Zhao, Y., & Lei, J. (2017). The incorrect usage of singular spectral analysis and discrete wavelet transform in hybrid models to predict hydrological time series. *Journal of Hydrology*, *552*, 44–51. https://doi.org/10.1016/j.jhydrol.2017.06.019

Epting, J., Huggenberger, P., Radny, D., Hammes, F., Hollender, J., Page, R. M., Weber, S., Banninger, D., & Auckenthaler, A. (2018). Spatiotemporal scales of river-groundwater interaction - the role of local interaction processes and regional groundwater regimes. *Science of the Total Environment*, *618*, 1224–1243. https://doi.org/10.1016/j.scitotenv.2017.09.219

Erickson, M. L., Yager, R. M., Kauffman, L. J., & Wilson, J. T. (2019). Drinking water quality in the glacial aquifer system, northern USA. *Science of the Total Environment*, *694*, 133735. https://doi.org/10.1016/j.scitotenv.2019.133735

Evans, C., & Davies, T. D. (1998). Causes of concentration/discharge hysteresis and its potential as a tool for analysis of episode hydrochemistry. *Water Resources Research*, *34*(1), 129–137.

Farge, M. (1992). Wavelet transforms and their application to turbulence. *Annual Review of Fluid Mechanics*, *24*, 395–457.

Ferreira, R. V., Cerqueira, M. A., de Melo, M. T., de Figueiredo, D. R., & Keizer, J. J. (2010). Spatial patterns of surface water quality in the Cértima River basin, Central Portugal. *Journal of Environmental Monitoring*, *12*(1), 189–199. https://doi.org/10.1039/b914409a

Fleming, S. W., Lavenue, A. M., Aly, A. H., & Adams, A. (2002). Practical applications of spectral analysis to hydrologic time series. *Hydrological Processes*, *16*, 565–574. https://doi.org/10.1002/hyp.523

Gandy, C. J., Smith, J. W. N., & Jarvis, A. P. (2007). Attenuation of mining-derived pollutants in the hyporheic zone: A review. *Science of the Total Environment*, *373*, 435–446. https://doi.org/10.1016/j.scitotenv.2006.11.004

Grinsted, A., Moore, J. C., & Jevrejeva, S. (2004). Application of the cross wavelet transform and wavelet coherence to geophysical time series. *Nonlinear Processes in Geophysics*, *11*, 561–566.

Guin, A., & Ritzi, R. W. (2008). Studying the effect of correlation and finite-domain size on spatial continuity of permeable sediments. *Geophysical Research Letters*, *35*, 1–7. https://doi.org/10.1029/2007GL032717

Harvey, J. W., & Bencala, K. E. (1993). The effect of streambed topography on surface-subsurface water exchange in mountain catchments. *Water Resources Research*, *29*(1), 89–98.

Harvey, J. W., Wagner, B. J., & Bencala, K. E. (1996). Evaluating the reliability of the stream tracer approach to characterize stream-subsurface water exchange. *Water Resources Research*, *32*(8), 2441–2451.

Heinz, J., Kleineidam, S., Teutsch, G., & Aigner, T. (2003). Heterogeneity patterns of quaternary glaciofluvial gravel bodies (SW-Germany): Application to hydrogeology. *Sedimentary Geology*, *158*, 1–23. https://doi.org/10.1016/S0037-0738(02)00239-7

Johnson, T. D., & Belitz, K. (2017). Domestic well locations and populations served in the contiguous U.S.: 1990. *Science of the Total Environment*, *607-608*, 658–668. https://doi.org/10.1016/j.scitotenv.2017.07.018

Jussel, P. (1989). Stochastic description of typical inhomogeneities of hydraulic conductivity in fluvial gravel deposits. In H. E. Kobus & W. Kinzelbach (Eds.), *Contaminant transport in groundwater: proceedings of the International Symposium on Contaminant Transport in Groundwater*, Stuttgart, 4-6 April 1986 (pp. 221–228). A.A. Balkema.

Klingbeil, R., Kleineidam, S., Asprion, U., Aigner, T., & Teutsch, G. (1999). Relating lithofacies to hydrofacies: Outcrop-based hydrogeological characterization of quaternary gravel deposits. *Sedimentary Geology*, *129*, 299–310.

Kobayashi, D., Ishii, Y., & Kodama, Y. (1999). Stream temperature, specific conductance and runoff process in mountain watersheds. *Hydrological Processes*, *13*, 865–876.

Levy, J., Birck, M. D., Mutiti, S., Kilroy, K. C., Windeler, B., Idris, O., & Allen, L. N. (2011). The impact of storm events on a riverbed system and its hydraulic conductivity at a site of induced infiltration. *Journal of Environmental Management*, *92*, 1960–1971. https://doi.org/10.1016/j.jenvman.2011.03.017

Lewandowski, J., Putschew, A., Schwesig, D., Neumann, C., & Radke, M. (2011). Fate of organic micropollutants in the hyporheic zone of a eutrophic lowland stream: Results of a preliminary field study. *Science*

of the Total Environment, *409*, 1824–1835. https://doi.org/10.1016/j.scitotenv.2011.01.028

Liu Y., Wallace C. D., Zhou Y., Ershadnia R., Behzadi F., Dwivedi D., Xue L., & Soltanian M. R. (2020). Influence of streambed heterogeneity on hyporheic flow and sorptive solute transport. *Water*, *12*(6), 1547. http://dx.doi.org/10.3390/w12061547

Lunt, I. A., & Bridge, J. S. (2004). Evolution and deposits of a gravelly braid bar, Sagavanirktok River, Alaska. *Sedimentology*, *51*, 415–432. https://doi.org/10.1111/j.1365-3091.2004.00628.x

Lunt, I. A., & Bridge, J. S. (2007). Formation and preservation of open-framework gravel strata in unidirectional flows. *Sedimentology*, *54*, 71–87. https://doi.org/10.1111/j.1365-3091.2006.00829.x

Lunt, I. A., Bridge, J. S., & Tye, R. S. (2004). Development of a 3-D depositional model of Braided-River gravels and sands to improve aquifer characterization. In *In Aquifer Characterization* (Vol. 80). SEPM Society for Sedimentary Geology. https://doi.org/10.2110/pec.04.80.0139

Martinez, J. L., Raiber, M., & Cox, M. E. (2015). Assessment of groundwater-surface water interaction using long-term hydrochemical data and isotope hydrology: Headwaters of the Condamine River, Southeast Queensland, Australia. *Science of the Total Environment*, *536*, 499–516. https://doi.org/10.1016/j.scitotenv.2015.07.031

Miall, A. D. (1996). *The Geology of Fluvial Deposits: Sedimentary Facies, Basin Analysis, and Petroleum Geology*. Berlin, Heidelberg: Springer. https://doi.org/10.1007/978-3-662-03237-4

Mutiti, S., & Levy, J. (2010). Using temperature modeling to investigate the temporal variability of riverbed hydraulic conductivity during storm events. *Journal of Hydrology*, *388*, 321–334. https://doi.org/10.1016/j.jhydrol.2010.05.011

Norris, S. E., & Spieker, A. M. (1966). *Ground-Water Resources of The Dayton Area*. Ohio: Ohio Department of Natural Resources, Division of Water.

Palmer, C. D., & Nadon, R. L. (1986). A radial injection tracer experiment in a confined aquifer, Scarborough, Ontario, Canada. *Groundwater*, *24*(3), 322–331. https://doi.org/10.1111/j.1745-6584.1986.tb01008.x

Peralta-Maraver, I., Reiss, J., & Robertson, A. L. (2018). Interplay of hydrology, community ecology and pollutant attenuation in the hyporheic zone. *Science of the Total Environment*, *610-611*, 267–275. https://doi.org/10.1016/j.scitotenv.2017.08.036

Pilgrim, D. H., Huff, D. D., & Steele, T. D. (1979). Use of specific conductance and contact time relations for separating flow components in storm runoff. *Water Resources Research*, *15*(2), 329–339.

Plummer, L. N., Busenberg, E., Bohlke, J. K., Nelms, D. L., Michel, R. L., & Schlosser, P. (2001). Groundwater residence times in Shenandoah National Park, blue Ridge Mountains, Virginia, USA: A multi-tracer approach. *Chemical Geology*, *179*, 93–111.

Ritzi, R. W., Jr., Jayne, D. F., Zahradnik, A. J., Jr., Field, A. A., & Fogg, G. E. (1994). Geostatistical modeling of heterogeneity in Glaciofluvial, Buried-Valley aquifers. *Groundwater*, *32*(4), 666–674. https://doi.org/10.1111/j.1745-6584.1994.tb00903.x

Ritzi, R. W., Jr., Dominic, D. F., Slesers, A. J., Greer, C. B., Reboulet, E. C., Telford, J. A., Masters, R. W., Klohe, C. A., Bogle, J. L., & Means, B. P. (2000). Comparing statistical models of physical heterogeneity in buried-valley aquifers. *Water Resources Research*, *36*(11), 3179–3192.

Ritzi, R. W., Dai, Z., Dominic, D. F., & Rubin, Y. N. (2002). Spatial structure of permeability in relation to hierarchical sedimentary architecture in buried-valley aquifers: centimeter to kilometer scales. bridging the gap between measurement and modeling in heterogeneous media. *International Groundwater Symposium*.

Runkel, R. L. (1998). One-dimensional transport with inflow and storage (OTIS): A solute transport model for streams and rivers.

Sang, Y.-F., Wang, Z., & Liu, C. (2012). Period identification in hydrologic time series using empirical mode decomposition and maximum entropy spectral analysis. *Journal of Hydrology*, *424-425*, 154–164. https://doi.org/10.1016/j.jhydrol.2011.12.044

Sawyer, A. H., Kaplan, L. A., Lazareva, O., & Michael, H. A. (2014). Hydrologic dynamics and geochemical responses within a floodplain aquifer and hyporheic zone during hurricane Sandy. *Water Resources Research*, *50*, 4877–1892. https://doi.org/10.1002/2013WR015101

Schaefli, B., Maraun, D., & Holschneider, M. (2007). What drives high flow events in the Swiss Alps? Recent developments in wavelet spectral analysis and their application to hydrology. *Advances in Water Resources*, *30*, 2511–2525. https://doi.org/10.1016/j.advwatres.2007.06.004

Schilling, K. E., Li, Z., & Zhang, Y.-K. (2006). Groundwater-surface water interaction in the riparian zone of an incised channel, Walnut Creek, Iowa. *Journal of Hydrology*, *327*, 140–150. https://doi.org/10.1016/j.jhydrol.2005.11.014

Schuite, J., Flipo, N., Massei, N., Rivi è re, A., & Baratelli, F. (2019). Improving the spectral analysis of hydrologic signals to efficiently constrain watershed properties. *Water Resources Research*, *55*(5), 4043–4065. https://doi.org/10.1029/2018WR024579

Smith, E. A., & Capel, P. D. (2018). Specific conductance as a tracer of preferential flow in a subsurface-drained field. *Vadose Zone Journal*, *17*, 1–13. https://doi.org/10.2136/vzj2017.11.0206

Soltanian, M. R., & Ritzi, R. W. (2014). A new method for analysis of variance of the hydraulic and reactive attributes of aquifers as linked to hierarchical and multiscaled sedimentary architecture. *Water Resources Research*, *50*(12), 9766–9776. https://doi.org/10.1002/2014WR015468

Spieker, A. M. (1968). Ground-water hydrology and geology of the lower great Miami River valley Ohio.

Stauffer, D., & Aharony, A. (1994). *Introduction to Percolation Theory: Revised Second Edition* (2nd ed.). Taylor & Francis.

Stollenwerk, K. G., & Grove, D. B. (1987). Natural-gradient tracer test in sand and gravel: Nonconservative transport of molybdenum.

Titzel, C. S. (1997). Quantification of the permeability distribution within sand and gravel lithofacies in a southern portion of the Miami Valley aquifer Wright State University.

Trauth, N., Schmidt, C., Vieweg, M., Oswald, S. E., & Fleckenstein, J. H. (2015). Hydraulic controls of in-stream gravel bar hyporheic exchange and reactions. *Water Resources Research*, *51*, 2243–2263. https://doi.org/10.1002/2014WR015857

Wallace C. D., Sawyer A. H., & Barnes R. T. (2019). Spectral analysis of continuous redox data reveals geochemical dynamics near the stream–aquifer interface. *Hydrological Processes*, *33*(3), 405–413. http://dx.doi.org/10.1002/hyp.13335.

Wallace, C. D., Sawyer, A. H., Barnes, R. T., Soltanian, M. R., Gabor, R. S., Wilkins, M. J., & Moore, M. T. (2020a). A model analysis of the tidal engine that drive nitrogen cycling in coastal riparian aquifers. *Water Resources Research*, *56*(4), 1–18. https://doi.org/10.1029/2019WR025662

Wallace, C. D., Sawyer, A. H., Soltanian, M. R., & Barnes, R. T. (2020b). Nitrate removal within heterogeneous riparian aquifers under tidal influence. *Geophysical Research Letters*, *47*(10), 1–11. https://doi.org/10.1029/2019GL085699

Warner, K. L., & Ayotte, J. D. (2014). *Water quality in the glacial aquifer system, northern United States, 1993–2009*. U.S. Geological Survey.

Wojnar, A. J., Mutiti, S., & Levy, J. (2012). Assessment of geophysical surveys as a tool to estimate riverbed hydraulic conductivity. *Journal of Hydrology*, *482*, 40–56. https://doi.org/10.1016/j.jhydrol.2012.12.018

Wondzell, S. M., & Swanson, F. J. (1996). Season and storm dynamics of the hyporheic zone of a 4th-order mountain stream. II: Nitrogen cycling. *Journal of the North American Benthological Society*, *15*(1), 20–34. https://doi.org/10.2307/1467430

Yager, R. M., Kauffman, L. J., Soller, D. R., Haj, A. E., Heisig, P. M., Buchwald, C. A., Westenbroek, S. M., & Reddy, J. E. (2019). Characterization and occurrence of confined and unconfined aquifers in quaternary sediments in the glaciated conterminous United States.

Zhou, Y., Ritzi, R. W., Soltanian, M. R., & Dominic, D. F. (2014). The influence of streambed heterogeneity on Hyporheic flow in gravelly Rivers. *Groundwater*, *52*(2), 206–216. https://doi.org/10.1111/gwat.12048

Zimmer, M. A., & Lautz, L. K. (2014). Temporal and spatial response of hyporheic zone geochemistry to a storm event. *Hydrological Processes*, *28*, 2324–2337. https://doi.org/10.1002/hyp.9778

SUPPORTING INFORMATION

Additional supporting information may be found online in the Supporting Information section at the end of this article.

How to cite this article: Wallace CD, Soltanian MR. Surface water-groundwater exchange dynamics in buried-valley aquifer systems. *Hydrological Processes*. 2021;35:e14066. https://doi.org/10.1002/hyp.14066